

Variable-kinematic finite beam elements for geometrically nonlinear dynamic analyses

Original

Variable-kinematic finite beam elements for geometrically nonlinear dynamic analyses / Azzara, Rodolfo; Filippi, Matteo; Pagani, Alfonso. - In: MECHANICS OF ADVANCED MATERIALS AND STRUCTURES. - ISSN 1537-6494. - ELETTRONICO. - (2022), pp. 1-9. [10.1080/15376494.2022.2091185]

Availability:

This version is available at: 11583/2971914 since: 2022-09-30T14:58:55Z

Publisher:

Taylor and Francis

Published

DOI:10.1080/15376494.2022.2091185

Terms of use:

This article is made available under terms and conditions as specified in the corresponding bibliographic description in the repository

Publisher copyright

Taylor and Francis preprint/submitted version

This is an Author's Original Manuscript of an article published by Taylor and Francis in MECHANICS OF ADVANCED MATERIALS AND STRUCTURES on 2022, available at <http://www.tandfonline.com/10.1080/15376494.2022.2091185>

(Article begins on next page)

Variable-kinematic finite beam elements for geometrically nonlinear dynamic analyses

R. Azzara^{1*}, M. Filippi^{1†}, A. Pagani^{1‡}

¹ Department of Mechanical and Aerospace Engineering, Politecnico di Torino
Corso Duca degli Abruzzi 24, 10129 Torino, Italy.

Abstract: *This paper investigates the dynamic nonlinear response of three-dimensional structures using variable-kinematics finite beam elements obtained with the Carrera Unified Formulation. The formalism enables one to consider the three-dimensional form of displacement-strain relations and constitutive law. The deformation mechanisms and the associated couplings are described consistently with the selected kinematic model. The Hilbert-Hughes-Taylor method and the iterative Newton-Raphson scheme are adopted to solve the motion equations derived in a total Lagrangian scenario. Various models have been obtained by using Taylor- and Lagrange-like expansions. The capabilities of the beam elements are assessed considering isotropic, homogeneous structures with compact and thin-walled sections.*

Keywords: Nonlinear structural dynamics; Carrera Unified Formulation; One-dimensional (1D) beam model; Geometrical nonlinearity; Implicit time integration; Newmark method; HHT- α method.

1 Introduction

Beam formulations are practical tools for idealizing various structures such as airplane wings, helicopter and wind turbine blades, flexible parts of spacecraft and satellites, robot arms, bridges, and high-rise buildings. The one-dimensional approach is adopted to perform strength and dynamic analyses to predict the structure's behavior under specific working conditions. Among the various applications where these models are used, the study of transient responses of deformable and slender components that exhibit large displacements and rotations has gained, over the years, significant interest [1].

One of the most prominent approaches used to solve geometrically nonlinear one-dimensional (1D) problems was the development of the so-called geometrically exact theories, whose first examples can be found in the pioneering works by Reissner [2] and Antman [3]. These theories are being defined *exact* because the kinetic and kinematic relations are consistently derived from the three-dimensional (3D) theory. Among others, Simo and Vu-Quoc provided influential contributions in this context. First, Simo [4] derived the deformation map of a beam with respect to a fixed reference system by utilizing a position vector and an orthogonal tensor as a measure of the cross-section rotation. Then, Simo and Vu-Quoc [5, 6] developed the associated finite element (FE) formulation and an update procedure for calculating the (infinitesimal) rotational changes along the beam axis. The quaternion parameters were introduced to describe the section rotation and avoid singularities. Later, different parametrizations of the rotational field were proposed by Cardona and Geradin [7], Ibrahimbegović *et al.* [8], Jelenić *et al.* [9, 10], and Ritto-Corrêa and Camotin [11].

*PhD student. E-mail: rodolfo.azzara@polito.it

†Assistant Professor. E-mail: matteo.filippi@polito.it

‡Associate professor. E-mail: alfonso.pagani@polito.it

An alternative approach for formulating geometrically nonlinear beam theories is the corotational method. The basic idea is to describe the nonlinear deformation as a combination of two contributions: the first due to a pure rigid body motion and the second due to small elastic deformations measured with respect to a local *corotated* reference system. Belytschko *et al.* [12, 13] were among the first to adopt the corotational strategy within the FE framework to perform static and transient analyses. Many other contributions have been then proposed, especially for the computational efficiency of the method, e.g., [14, 15, 16]. Felippa and Haugen provided a comprehensive overview on derivation aspects of corotational finite elements in Ref. [17].

A central issue in developing nonlinear 3D beam formulations concerns the treatment of the rotational field because of its noncommutative nature. Shabana [18, 19, 20] developed finite elements based on the so-called *absolute nodal coordinate formulation*. The method does not require independent interpolations of displacements and rotations since it allows the description of the beam element configuration by using the position and slope vectors of elemental nodes. The main advantage is that the inertial forces are merely given by the product between a constant mass matrix and the acceleration vector; therefore, no additional matrices are required to trace the rigid body motion. Nevertheless, detailed studies [21, 22] revealed that beam elements based on the absolute nodal coordinate formulation are computationally more intensive and less accurate than those obtained with the geometrically exact approach.

From the proposed literature review, although not comprehensive (see, for more details, Ref. [23]), we can infer that the derivation of nonlinear 1D formulations is not a simple task. Most models rely on simplified constitutive relations and assume rigid cross-sections to lessen the problem complexity. Furthermore, the extension of nonlinear theories to either thin-walled or composite structures is not straightforward as in the geometrically linear case [24, 25, 16].

The present work investigates the nonlinear dynamic response of beam-like structures through variable kinematics one-dimensional finite elements. The Carrera Unified Formulation (CUF) is adopted to derive the equations of motion associated with arbitrary structural theories in a total Lagrangian scenario. The strain-displacement relations and the linear constitutive model are three-dimensional regardless of which kinematics is adopted. Thus, the Green-Lagrange strain tensor and the elastic coefficients matrix encompass all terms. The nonlinear CUF-based beam elements have been previously assessed for static/stability [26, 27, 28] and vibration [29, 30, 31] problems. The solution of nonlinear equations is computed with a Newton-Raphson iterative strategy and integrated in time with the Hilber-Hughes-Taylor (HHT)- α method. The work is organized as follows: (i) first, CUF is briefly introduced in Section 2, focusing the interest on the geometrically nonlinear formulation; (ii) then, Section 3 describes the nonlinear dynamic formulation, illustrating the solving scheme; (iii) next, Section 4 presents some numerical results, comparing them with solutions available in the literature or obtained with commercial FE codes; (iv) finally, the main conclusions are reported in Section 5.

2 Unified formulation of geometrically nonlinear beam theory

According to the unified formulation and considering a Cartesian reference system (x, y, z) , the three-dimensional displacement field \mathbf{u} of a generic point belonging to a structure with the cross-section lying on the $x - z$ plane and the longitudinal axis aligned with the y -direction is written as

$$\mathbf{u}(x, y, z; t) = F_\tau(x, z) \mathbf{u}_\tau(y; t) \quad \tau = 1, \dots, M \quad (1)$$

where F_τ are arbitrary functions of $x - z$ coordinates, \mathbf{u}_τ is the vector of generalized displacements dependent on time t and the y -coordinate, M is the number of functions F_τ included into the kinematic expansion, and the repeated index τ denotes summation. If the finite element method is employed to approximate the generalized coordinates through the shape functions $N_i(y)$ and the vector of the generalized nodal coordinates $\mathbf{q}(t)$, the resulting equation becomes

$$\mathbf{u}(x, y, z; t) = F_\tau(x, z) N_i(y) \mathbf{q}_{\tau i}(t) \quad i = 1, \dots, nn_{el} \quad \tau = 1, \dots, M \quad (2)$$

The subscript i varies from 1 to the number of structural nodes of a single finite element nn_{el} . Linear, quadratic, and cubic finite beam element formulations are obtained with two (B2), three (B3), and four nodes (B4), respectively (see Ref. [32]). The number and type of cross-section functions are free parameters of the analysis; therefore, various structural theories can be conceived by selecting them properly. In this work, Lagrange- and Taylor-type expansions are utilized to approximate the displacement field over the structure's cross-section. The Lagrange structural models are obtained by discretizing the section into an arbitrary number of two-dimensional domains (also called Lagrange-type elements) delimited by some points (also called section nodes). The number of these points determines the order of kinematic (Lagrangian) functions (F_τ) of the element. Bi-linear (L4), bi-quadratic (L9), and bi-cubic (L16) elements are obtained with four, nine, and sixteen points, respectively. For each point, the generalized coordinate vector consists of three terms representing the translations of the sectional node itself. Instead, when the Taylor-type approach is used, the displacement components are written as an arbitrary-order power series of the cross-section coordinates ($x - z$). The first-order Taylor-like expansion (TE1), for example, consists of nine terms. Three of them (one for each displacement component) represent the rigid translations of the structural node, and the remaining six are related to the slopes of the displacement components with respect to the x and z directions. Thus, one of the main differences between the two types of expansions is the nature of the generalized coordinates. Likewise 3D FE models, the beam formulations based on the Lagrange kinematics allow the description of the structure's motion through the displacements of some nodes. The Taylor-based kinematics enables the structure deformation to be obtained by interpolating the generalized nodal coordinates (translations, rotations, and higher-order terms) within each element. This feature presents similarities with the absolute nodal coordinate concept. The geometrically nonlinear FE governing equations are obtained according to a total Lagrangian formulation by including all components of the Green-Lagrangian strain tensor. Through the use of the linear and nonlinear differential operators, \mathbf{b}_l and \mathbf{b}_{nl} , and the stiffness matrix for linear elastic materials, \mathbf{C} , the strain-displacement relation, and the constitutive law are

$$\begin{aligned} \boldsymbol{\epsilon} &= \boldsymbol{\epsilon}_l + \boldsymbol{\epsilon}_{nl} = (\mathbf{b}_l + \mathbf{b}_{nl})\mathbf{u} \\ \boldsymbol{\sigma} &= \mathbf{C}\boldsymbol{\epsilon} \end{aligned} \quad (3)$$

It should be underlined that the extension to nonlinear constitutive models is straightforward [33, 34]. The substitution of Eqs. 2 and 3 into the principle of virtual work enables the virtual variations of both strain energy (δL_{int}) and works done by inertial forces (δL_{ine}) and external loads (δL_{ext}) to be expressed in the CUF formalism

$$\begin{aligned} \delta L_{int} &= \delta \mathbf{q}_{sj}^T \mathbf{K}_s^{ij\tau s} \mathbf{q}_{\tau i} \\ \delta L_{ine} &= \delta \mathbf{q}_{sj}^T \mathbf{M}^{ij\tau s} \ddot{\mathbf{q}}_{\tau i} \\ \delta L_{ext} &= \delta \mathbf{q}_{sj}^T \mathbf{F}^{sj} \end{aligned} \quad (4)$$

The 3-by-3 matrices $\mathbf{K}_s^{ij\tau s}$ and $\mathbf{M}^{ij\tau s}$ and the 3-by-1 vector \mathbf{F}^{sj} are the so-called *fundamental nuclei* of the secant stiffness matrix, the mass matrix, and the loading vector, respectively. The expressions of their components are invariant, and they can be computed by permuting the indexes τ , i, s , and j . The latter two are used for the displacements' virtual variations and have the same bounds of τ and i . Removing the indexes for the assembled matrices and vector, the resulting nonlinear equations of motion are

$$\mathbf{M}\ddot{\mathbf{q}}(t) + \mathbf{K}_s(\mathbf{q})\mathbf{q}(t) = \mathbf{F}(t) \quad (5)$$

The Newton-Raphson method and an implicit step-by-step time integration scheme are used in this work to solve Eq. 5. Omitting the second-order terms and taking into account that the mass matrix

is constant, the tangent stiffness matrix deriving from the linearization of the residual nodal forces for a dynamic problem has the following form

$$\begin{aligned} \delta(\delta L_{int} + \delta L_{ine} - \delta L_{ext}) &= \delta \mathbf{q}_{sj}^T (\mathbf{K}_0^{ij\tau s} + \mathbf{K}_{T1}^{ij\tau s}) \delta \mathbf{q}_{\tau i} + \delta \mathbf{q}_{sj}^T \mathbf{K}_\sigma^{ij\tau s} \delta \mathbf{q}_{\tau i} + \delta \mathbf{q}_{sj}^T \mathbf{M}^{ij\tau s} \delta \ddot{\mathbf{q}}_{\tau i} \\ &= \delta \mathbf{q}_{sj}^T \mathbf{K}_T^{ij\tau s} \delta \mathbf{q}_{\tau i} + \delta \mathbf{q}_{sj}^T \mathbf{M}^{ij\tau s} \delta \ddot{\mathbf{q}}_{\tau i} = 0 \end{aligned} \quad (6)$$

The *fundamental nucleus* of matrix $\mathbf{K}_T^{ij\tau s}$ can be found in Ref. [27]. Moreover, it should be underlined that the external loads are considered conservative; therefore the linearization of the virtual variation of external work is null.

3 The iterative solution algorithm

The Newmark method with $\beta = 0.25$ and $\gamma = 0.5$ (i.e. trapezoidal rule) can be employed to calculate the time response of structures undergoing large displacements and rotations. This algorithm is not dissipative and, therefore, does not determine an amplitude decay of the response. However, the trapezoidal rule, known to be unconditionally stable in the linear analysis, may become unstable in nonlinear dynamic analyses, especially when significantly large deformations and long-time responses are investigated. A strategy for preventing these instabilities is the development of solving algorithms with some numerical damping to suppress any spurious growth of high-frequency responses. In this work, the HHT- α method [35] is adopted mainly for the following two reasons: 1) the implementation is straightforward, and 2) one can modulate the dissipation property of the algorithm by selecting the time step and the value of the parameter α opportunely. Moreover, it should be highlighted that if $\alpha = 0$, the HHT- α scheme reduces to the Newmark algorithm. For completeness, the solving procedure is reported below.

1. Form stiffness \mathbf{K}_s and mass matrix \mathbf{M} ;
2. Set the initial conditions;
3. **For each time-step:**

- (a) Starting conditions:

$$\begin{aligned} \ddot{\mathbf{q}}_{t+\Delta t} &= 0 \\ \mathbf{q}_{t+\Delta t} &= \mathbf{q}_t + \dot{\mathbf{q}}_t \Delta t + [(1/2 - \beta) \ddot{\mathbf{q}}_t + \beta \ddot{\mathbf{q}}_{t+\Delta t}] \Delta t^2 \\ \dot{\mathbf{q}}_{t+\Delta t} &= \dot{\mathbf{q}}_t + [(1 - \gamma) \ddot{\mathbf{q}}_t + \gamma \ddot{\mathbf{q}}_{t+\Delta t}] \Delta t \end{aligned}$$

- (b) Form residual load vector $\mathbf{R}_{t+\Delta t}$:

$$\mathbf{R}_{t+\Delta t} = (1 + \alpha) \mathbf{F}_{t+\Delta t} - \alpha \mathbf{F}_t - (1 + \alpha) \mathbf{r}_{t+\Delta t} + \alpha \mathbf{r}_t - \mathbf{M} \ddot{\mathbf{q}}_{t+\Delta t}$$

in which \mathbf{r} represents the internal force.

- (c) Newton-Raphson iteration convergence:

- i. **while** $\|\mathbf{R}_{t+\Delta t}\| \geq Tol$ **do**
- ii. Calculate tangent stiffness matrix \mathbf{K}_T ;
- iii. Solve for incremental acceleration $\Delta \ddot{\mathbf{q}}_{t+\Delta t}$:

$$[(\mathbf{M} + \mathbf{K}_T \beta \Delta t^2 (1 + \alpha))] \Delta \ddot{\mathbf{q}}_{t+\Delta t} = \mathbf{R}_{t+\Delta t}$$

iv. Calculate new acceleration, velocity and displacement vectors:

$$\ddot{\mathbf{q}}_{t+\Delta t} = \ddot{\mathbf{q}}_{t+\Delta t} + \Delta \ddot{\mathbf{q}}_{t+\Delta t}$$

$$\dot{\mathbf{q}}_{t+\Delta t} = \dot{\mathbf{q}}_{t+\Delta t} + \Delta \dot{\mathbf{q}}_{t+\Delta t} \gamma \Delta t$$

$$\mathbf{q}_{t+\Delta t} = \mathbf{q}_{t+\Delta t} + \Delta \mathbf{q}_{t+\Delta t} \beta \Delta t^2$$

v. Calculate new residual load vector.

$$\mathbf{R}_{t+\Delta t} = (1 + \alpha)\mathbf{F}_{t+\Delta t} - \alpha\mathbf{F}_t - (1 + \alpha)\mathbf{r}_{t+\Delta t} + \alpha\mathbf{r}_t - \mathbf{M}\ddot{\mathbf{q}}_{t+\Delta t}$$

vi. **end while**

(d) Next time step.

The parameters α , $\beta = (1 - \alpha)^2/4$ and $\gamma = (1 - 2\alpha)/2$ control the accuracy, stability and numerical dissipation characteristics. As pointed out in Ref. [35], a value of $-1/3 \leq \alpha \leq 0$ is suggested to avoid unacceptable damping of low-frequency modes of the structural response.

4 Results

The first simulations concerned two cantilever square cross-section beams, whose dimensions, material properties, boundary and loading conditions are shown in Fig. 1. The length-to-thickness ratios (L/h) were 100 and 10 for *Case I* and *Case II*, respectively. The adopted mathematical models consisted of ten 4-node finite beam elements over the y -axis for both cases.

Figure 2 shows the deflections at the structure's mid-span calculated with the first-order shear deformation theory (TE1) and the Lagrange quadratic theory (1-L9). Moreover, two reference solutions obtained with the Nastran FE software are reported for comparison purposes. The 1D and 3D reference models consisted of 30 finite beam elements and $4 \times 30 \times 4$ 8-node brick elements, respectively. The time-step and the control parameter used in the analyses have been selected equal to $\Delta t = 0.004$ seconds and $\alpha = -0.05$.

The comparison revealed a significant agreement between the 1D-CUF solutions and the 3D reference curve in the considered time interval. Instead, after roughly 5 seconds, we can observe a moderate lag in the 1D reference curve and slight discrepancies in peaks amplitude. It should be highlighted that the 1D reference solution was convergent, although the corresponding number of degrees of freedom (d.o.f.) was the lowest. Nevertheless, the TE1 and the 1-L9 theories determined reductions of approximately 80% and 28% in the unknowns number compared to the 3D model.

For *Case II*, the dynamic response at the beam's tip with $\Delta t = 0.05$ seconds and $\alpha = -0.05$ was calculated by adopting linear (TE1 and 1-L4), quadratic (TE2 and 1-L9), and cubic (TE3) kinematic theories. The related curves are shown in Fig. 3, together with the results presented in Ref. [36] and a 3D FE solution. Contrary to what we observed for the previous configuration, the approaches led to different solutions due to the reduced slenderness ratio of the structure. First, linear and quadratic models have predicted consistent transient responses in the first 50 seconds, while the TE3 solution differs in the peaks' number and amplitude. Second, as time increases, the dynamic responses related to low-order expansions (TE1 and 1-L4) agree with the Nastran solution obtained with $2 \times 30 \times 2$ 8-node hexahedral elements, whilst the higher-order theories have provided larger deflections. Furthermore, we observed a difference in the oscillation period predicted by the TE3 expansion and those related to the other approaches in the first 100 seconds and a substantial agreement in the remaining interval. Lastly, the result presented by Boujelben and Ibrahimbegovic in Ref. [36] obtained with an advanced solid FE formulation slightly underestimated the amplitude oscillations. This mismatch can be ascribed to the coarse mesh and the different time-step used for the analysis.

Next, we investigated the dynamics of two deformable pendulums subjected to the gravity force ($P_z = \int_V dP_z dV$). Figure 4 shows the dimensions and mechanical properties of the configurations, named "Pendulum I" and "Pendulum II". The structures, modelled with ten 4-node beam elements, can elastically deform and rigidly rotate since they were hinged at one end. For all simulations, the used time-step was $\Delta t = 0.001$ seconds, while the value of the control parameter α remained unchanged with respect to the previous analyses ($\alpha = -0.05$). Figure 5 shows the positions of the central point at the free-ends. For Pendulum I, the various 1D-CUF models provided the same results, accurately reproducing the reference solution obtained with a nonlinear beam element based on the Euler-Bernoulli model proposed in Ref. [37]. Instead, it is possible to observe discrepancies between the models for the second configuration because of its higher flexibility. As the theory's order increases, the cross-section deformations due to the inertial effects were detected. These deformation mechanisms significantly affected the dynamic responses over time, as demonstrated in Fig. 6. Eventually, the dynamic response of the cantilever thin-walled rectangular beam illustrated in Fig. 7 was examined. The structure was subjected to a vertical force ($P_{z0} = 50$ kN) distributed on the top surface and constant in time. We reported the results obtained with the second-order Taylor-type kinematics (TE2) and a Lagrange model consisting of ten 9-node elements (10-L9), three for the top and bottom surface, respectively, and two for each lateral edge. Moreover, the finite element mesh consisted of fifteen 4-node elements along the span for all analyses. Figure 8 compares the geometrically linear and nonlinear dynamic responses calculated with the two kinematic models at the beam's tip.

The 10-L9 nonlinear solution significantly differs from the other results in both oscillation amplitude and period. These discrepancies were due to local instabilities occurring at the clamped root that determined a reduction of the structural stiffness. Such a softening effect can be detected if the kinematic model enables cross-sectional deformations to be described accurately. Figure 9 compares the nonlinear equilibrium curves with the linear ones at various locations along the beam's span. According to the 10-L9 solution, the top panel near the fixed end suddenly buckles when the load is approximately 15 kN. On the contrary, the nonlinear solution obtained with the second-order Taylor-type model strongly agreed with the linear predictions; indeed, no stiffness variation has been revealed in the considered load range. Figure 10 shows the deformed configurations and the axial stress distributions at $t = 0.3\bar{3}$ sec. and $L = 1.3\bar{3}$ m obtained with the nonlinear and linear formulations. The nonlinear solution shows that the bottom edge significantly deforms, and the top surface is subjected to a compressive-tensile stress state, contrary to what predicted by the linear result.

5 Conclusions

This paper explored the capabilities of variable-kinematic finite beam elements for the dynamic analysis of 3D structures undergoing large displacements and rotations. The equation of motion was derived in a total Lagrangian scenario using all terms of the Green-Lagrange strain tensor and the linear constitutive's law in a three-dimensional form. Taylor- and Lagrange-type expansions of various orders were adopted to define the displacement field of the finite elements. Regardless of which structural model was selected, the dynamic equilibrium of the structure was obtained by incrementing the generalized coordinate vector and the associated temporal derivatives by adopting an iterative Newton-Raphson procedure and the HHT- α method. The current approach was validated by considering results available in the literature and obtained with commercial software. As far as compact beam-like structures were concerned, the low-order 1D-CUF elements provided similar results to classical beam formulations with comparable computational efforts. Instead, when the dynamic response of highly-deformable structures was considered, the possibility of selecting the kinematic assumptions represented a valuable feature for detecting the cross-section deformations and local instabilities.

Declaration of Interest statement

The authors declare that they have no conflict of interest.

References

- [1] P.F. Pai. *Highly Flexible Structures: Modeling, Computation, and Experimentation*. 2007.
- [2] E. Reissner. On one-dimensional large-displacement finite-strain beam theory. *Studies in Applied Mathematics*, 52:87–95, June 1973.
- [3] Stuart S. Antman. Kirchhoff’s problem for nonlinearly elastic rods. *Quarterly of Applied Mathematics*, 32:221–240, 1974.
- [4] J. C. Simo. A finite strain beam formulation. the three-dimensional dynamic problem. part i. *Computer Methods in Applied Mechanics and Engineering*, 49:55–70, 1985.
- [5] Juan C Simo and Loc Vu-Quoc. A three-dimensional finite-strain rod model. part ii: Computational aspects. *Computer methods in applied mechanics and engineering*, 58(1):79–116, 1986.
- [6] JC Simo and L Vu-Quoc. The role of non-linear theories in transient dynamic analysis of flexible structures. *Journal of Sound and Vibration*, 119(3):487–508, 1987.
- [7] A. Cardona and M. Geradin. A beam finite element non-linear theory with finite rotations. *International Journal for Numerical Methods in Engineering*, 26:2403–2438, 1988.
- [8] Adnan Ibrahimbegovic, Francois Frey, and Ivica Kozar. Computational aspects of vector-like parametrization of three-dimensional finite rotations. *International Journal for Numerical Methods in Engineering*, 38:3653–3673, 1995.
- [9] G. Jelenic and M. Saje. A kinematically exact space finite strain beam model — finite element formulation by generalized virtual work principle. *Computer Methods in Applied Mechanics and Engineering*, 120:131–161, 1995.
- [10] G. Jelenić and M. A. Crisfield. Geometrically exact 3d beam theory: implementation of a strain-invariant finite element for statics and dynamics. *Computer Methods in Applied Mechanics and Engineering*, 171:141–171, 1999.
- [11] M. Ritto-Corrêa and D. Camotim. On the differentiation of the rodrigues formula and its significance for the vector-like parameterization of reissner-simo beam theory. *International Journal for Numerical Methods in Engineering*, 55:1005–1032, 2002.
- [12] T. Belytschko and B. J. Hsieh. Non-linear transient finite element analysis with convected co-ordinates. *International Journal for Numerical Methods in Engineering*, 7:255–271, 1973.
- [13] Ted Belytschko and Lawrence W. Glaum. Applications of higher order corotational stretch theories to nonlinear finite element analysis. *Computers and Structures*, 10:175–182, 1979.
- [14] C. C. Rankin and F. A. Brogan. An element independent corotational procedure for the treatment of large rotations. *Journal of Pressure Vessel Technology*, 108:165–174, 1986.
- [15] Thanh-Nam Le, Jean-Marc Battini, and Mohammed Hjiiaj. Corotational formulation for non-linear dynamics of beams with arbitrary thin-walled open cross-sections. *Computers and Structures*, 134:112–127, 2014.
- [16] A. Genoese, A. Genoese, A. Bilotta, and G. Garcea. A geometrically exact beam model with non-uniform warping coherently derived from the saint venant rod. *Engineering Structures*, 68:33–46, 2014.
- [17] C. A. Felippa and B. Haugen. A unified formulation of small-strain corotational finite elements: I. theory. *Computer Methods in Applied Mechanics and Engineering*, 194:2285–2335, 2005.

- [18] AA Shabana. Finite element incremental approach and exact rigid body inertia. *Journal of Mechanical Design*, 1996.
- [19] Ahmed A. Shabana and Refaat Y. Yakoub. Three dimensional absolute nodal coordinate formulation for beam elements: Theory. *Journal of Mechanical Design*, 123:606–613, 2001.
- [20] Refaat Y. Yakoub and Ahmed A. Shabana. Three dimensional absolute nodal coordinate formulation for beam elements: Implementation and applications. *Journal of Mechanical Design*, 123:614–621, 2001.
- [21] Ignacio Romero. A comparison of finite elements for nonlinear beams: the absolute nodal coordinate and geometrically exact formulations. *Multibody System Dynamics*, 20:51–68, 2008.
- [22] Olivier A. Bauchau, Shilei Han, Aki Mikkola, and Marko K. Matikainen. Comparison of the absolute nodal coordinate and geometrically exact formulations for beams. *Multibody System Dynamics*, 32:67–85, 2014.
- [23] Christoph Meier, Alexander Popp, and Wolfgang A. Wall. Geometrically exact finite element formulations for slender beams: Kirchhoff–love theory versus simo–reissner theory. *Archives of Computational Methods in Engineering*, 26:163–243, 2019.
- [24] Marco Borri and Teodoro Merlini. A large displacement formulation for anisotropic beam analysis. *Meccanica*, 21:30–37, 1986.
- [25] Mayuresh J. Patil and Dewey H. Hodges. Variable-order finite elements for nonlinear, fully intrinsic beam equations. *Journal of Mechanics of Material and Structures*, 6:479–493, 2011.
- [26] A. Pagani and E. Carrera. Large-deflection and post-buckling analyses of laminated composite beams by carrera unified formulation. *Composite Structures*, 170:40–52, 2017.
- [27] A. Pagani and E. Carrera. Unified formulation of geometrically nonlinear refined beam theories. *Mechanics of Advanced Materials and Structures*, 25(1):15–31, 2018.
- [28] A. Pagani, E. Carrera, and R. Augello. Evaluation of various geometrical nonlinearities in the response of beams and shells. *AIAA Journal*, 57(8):3524–3533, 2019.
- [29] M. Filippi, A. Pagani, and E. Carrera. Accurate nonlinear dynamics and mode aberration of rotating blades. *Journal of Applied Mechanics*, 85, 2018.
- [30] A. Pagani, R. Augello, and E. Carrera. Frequency and mode change in the large deflection and post-buckling of compact and thin-walled beams. *Journal of Sound and Vibration*, 432:88–104, 2018.
- [31] M. Filippi, A. Pagani, and E. Carrera. Three-dimensional solutions for rotor blades using high-order geometrical nonlinear beam finite elements. *Journal of the American Helicopter Society*, 64:1–10, 2019.
- [32] K.J. Bathe. *Finite element procedure*. Prentice Hall, Upper Saddle River, New Jersey, USA, 1996.
- [33] E. Carrera, A. Pagani, B. Wu, and M. Filippi. Large-deformation analysis of elastomeric structures by carrera unified formulation. In *ASME 2019 International Mechanical Engineering Congress and Exposition*, 2019.
- [34] A. Pagani and E. Carrera. Unified one-dimensional finite element for the analysis of hyperelastic soft materials and structures. *Mechanics of Advanced Materials and Structures*, pages 1–14, 2021.

- [35] H.M. Hilber, T.J.R. Hughes, and R.L. Taylor. Improved numerical dissipation for time integration algorithms in structural dynamics. *Earthquake Engineering & Structural Dynamics*, 5(3):283–292, 1977.
- [36] A. Boujelben and A. Ibrahimbegovic. Finite-strain three-dimensional solids with rotational degrees of freedom: non-linear statics and dynamics. *Advanced Modeling and Simulation in Engineering Sciences*, 4(1):1–24, 2017.
- [37] M. Sharifnia. A higher-order nonlinear beam element for planar structures by using a new finite element approach. *Acta Mechanica*, pages 1–17, 2022.

Figure

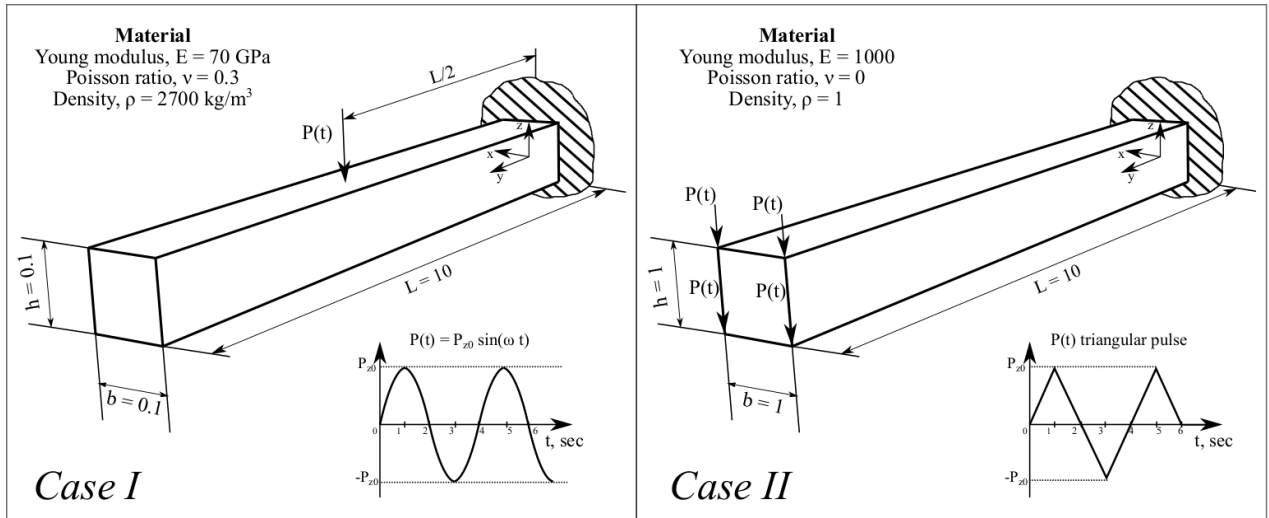


Figure 1: Geometry and loading conditions of the cantilever beam structures.

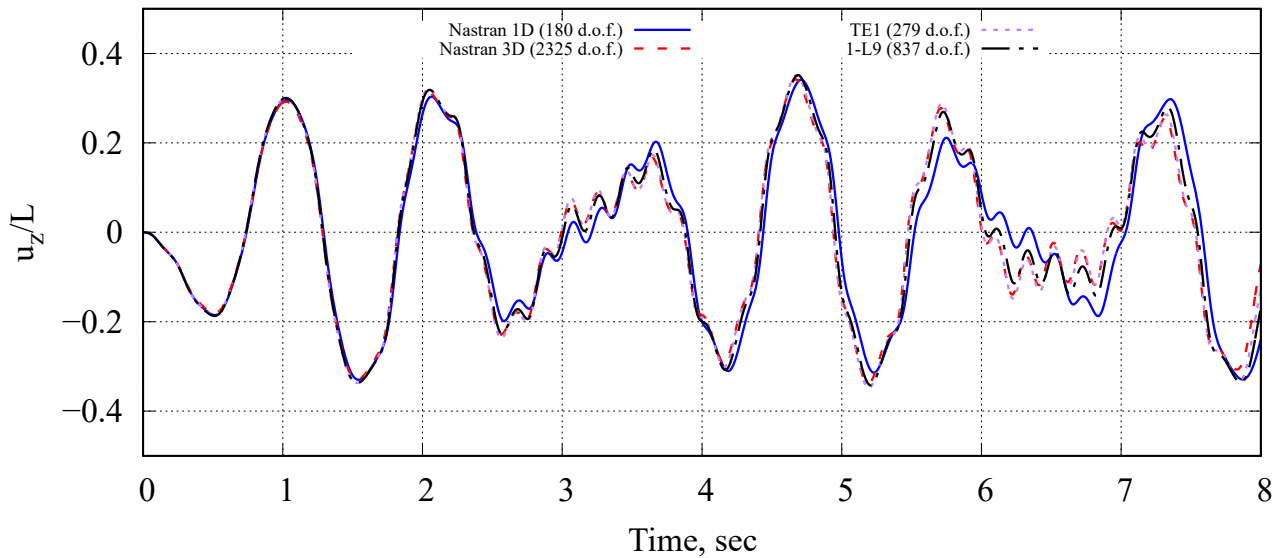


Figure 2: Transverse displacement vs. time at point $(0, L/2, 0)$ computed with various FE models. *Case I* of Fig. 1 with $P_{z0} = -25000 \text{ N}$, $\omega = 7 \text{ rad/s}$.

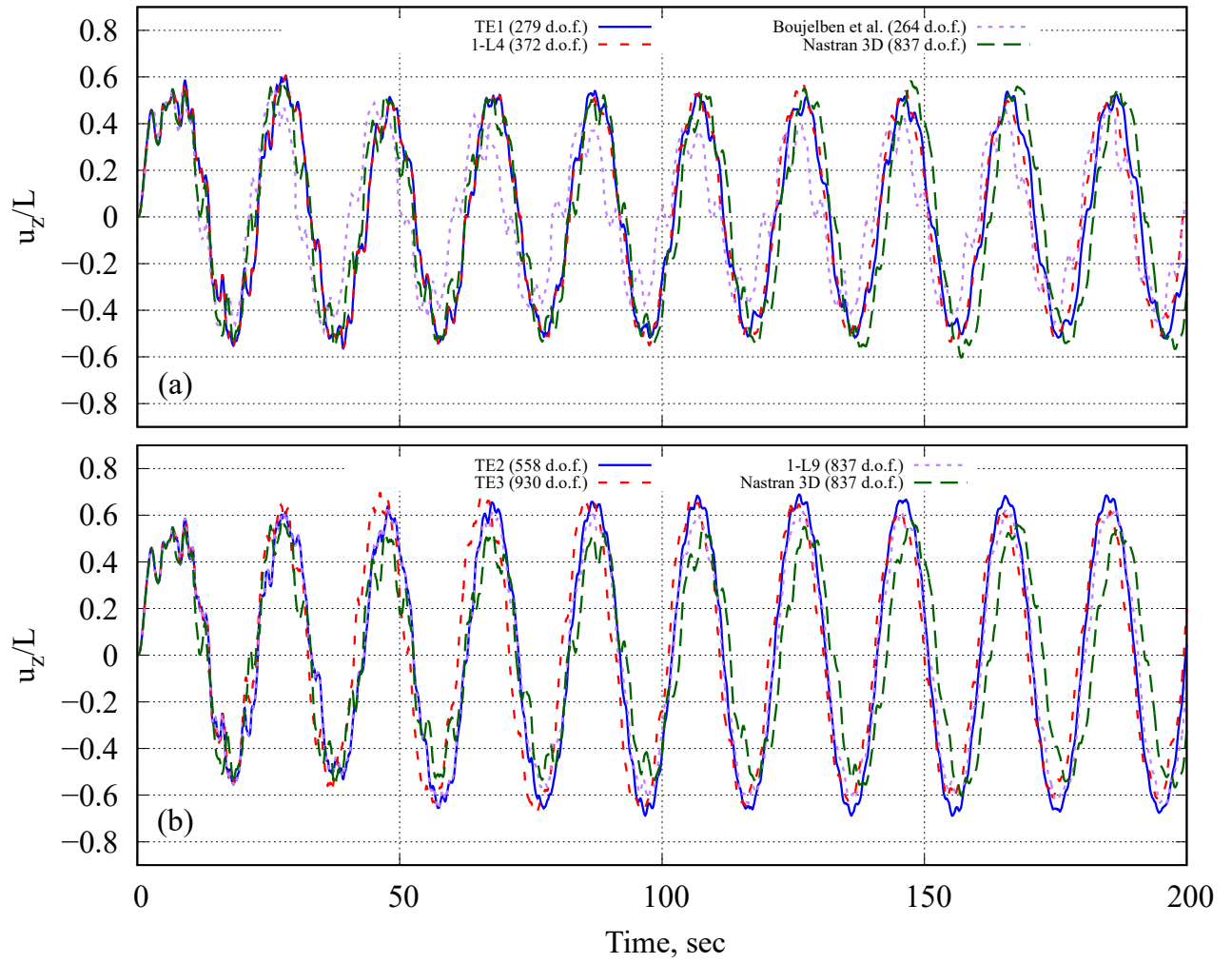


Figure 3: Transverse displacement vs. time at point $(0, L, 0)$ computed with various FE models. *Case II* of Fig. 1 with $P_{z0} = 2$ N.

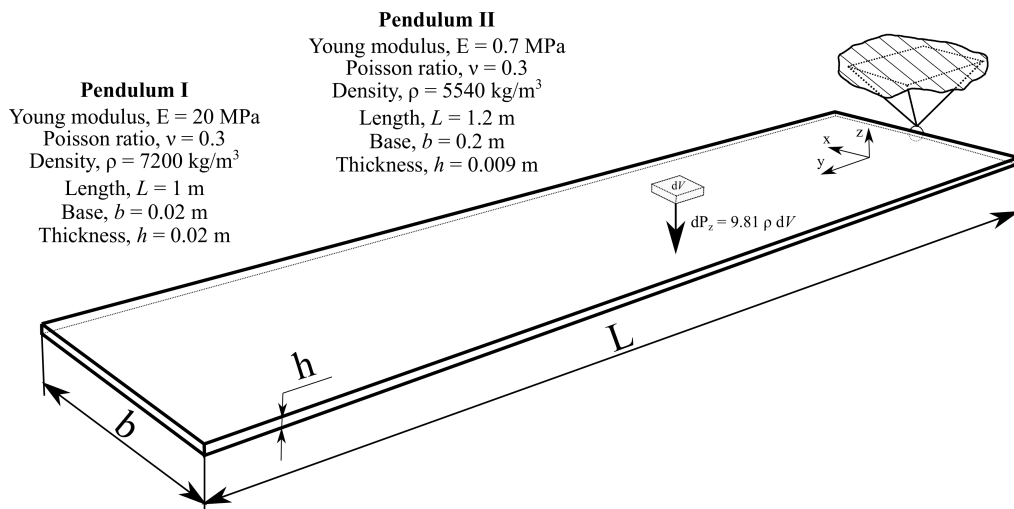


Figure 4: Geometry and loading conditions of the pendulums subjected to the gravity load.

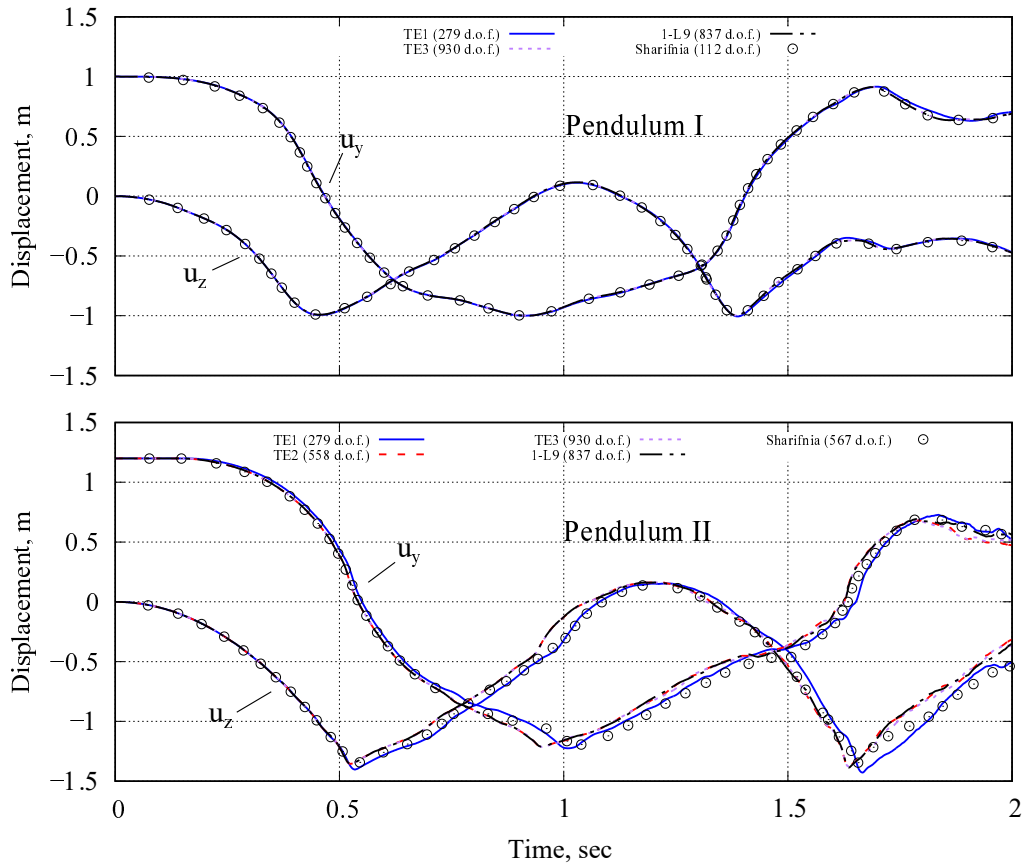


Figure 5: Positions of points at $(0, L, 0)$ calculated with various beam formulations.

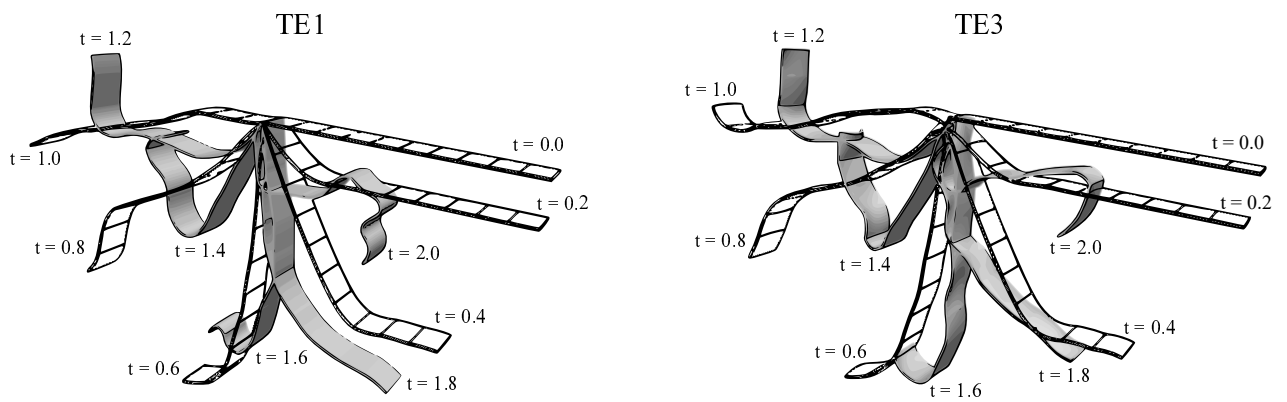


Figure 6: Motion of Pendulum II computed with two kinematic models.

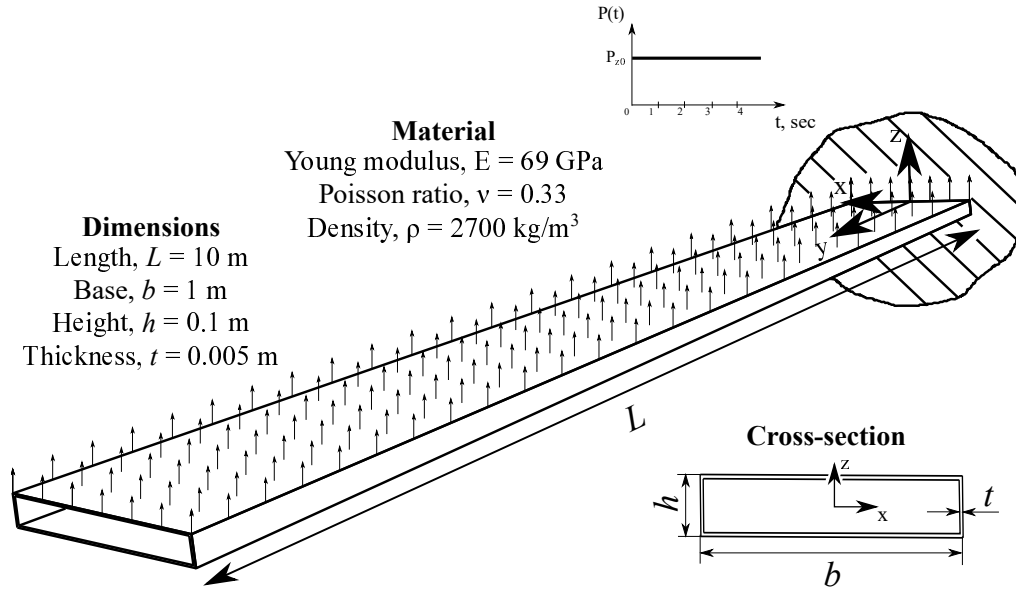


Figure 7: Geometry and material properties of the cantilever thin-walled beam.

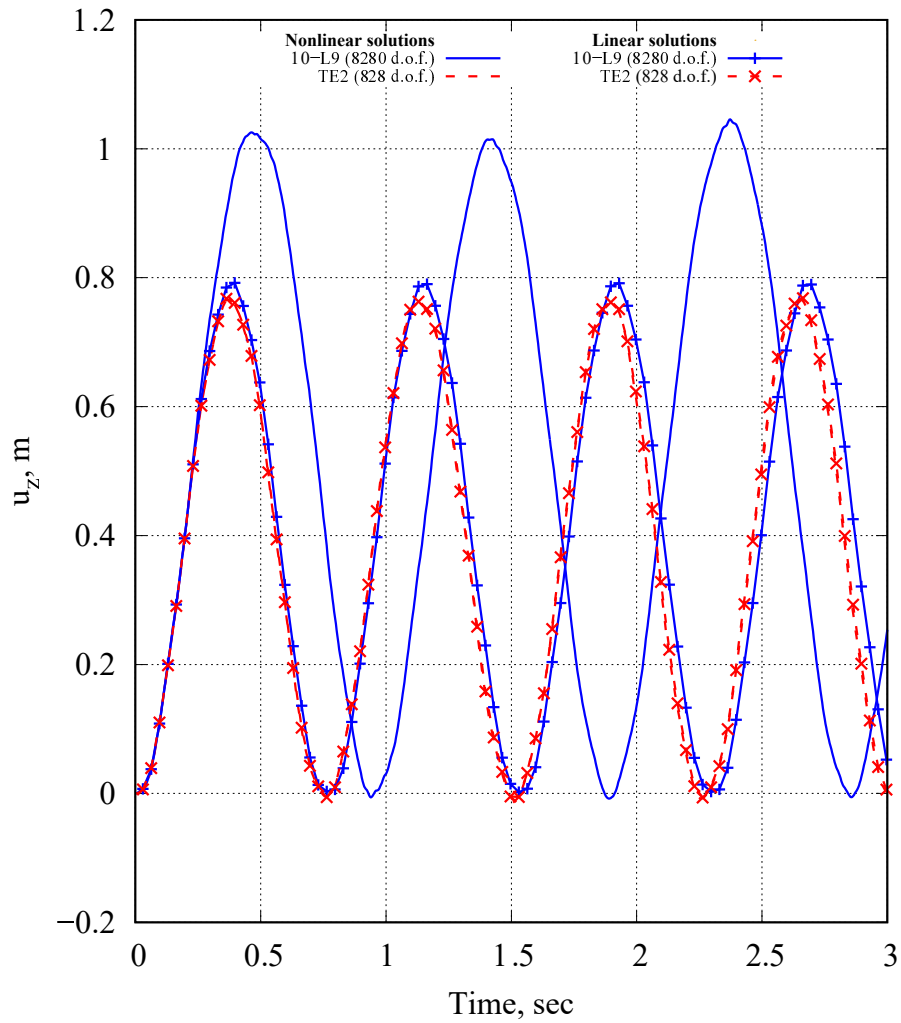


Figure 8: Geometrically linear and nonlinear transient responses of the thin-walled beam (see Fig. 7) calculated at $(0, L, h/2)$. Time step $\Delta t = 0.003\bar{3}$, $\alpha = -0.05$.

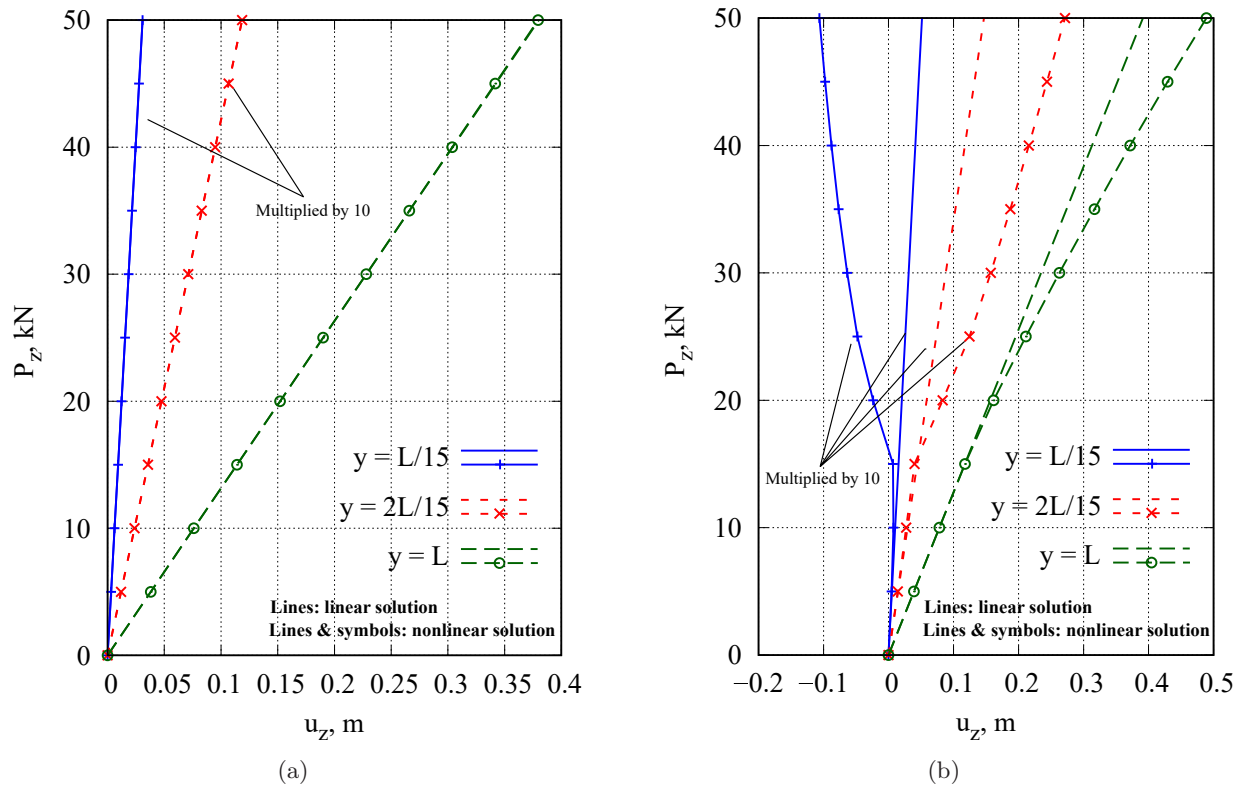


Figure 9: Linear and nonlinear equilibrium curves calculated at three locations along the thin-walled beam span $(0, y, h/2)$ of Fig. 7. Results obtained with the (a) TE2 and (b) 10-L9 models.

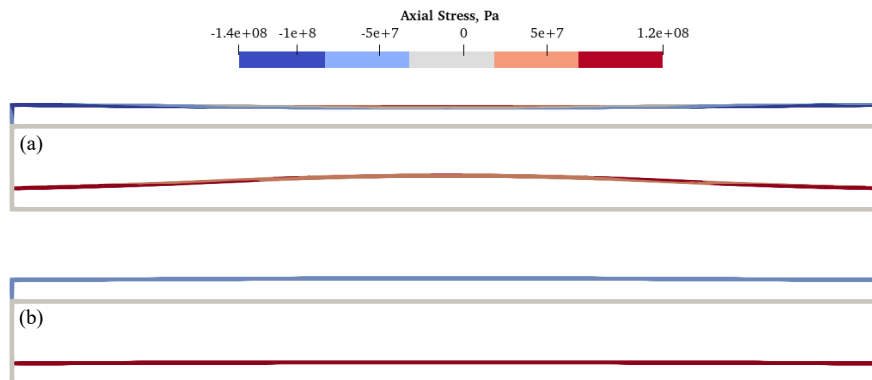


Figure 10: Axial stress distributions calculated with the 10-L9 model at $t = 0.33$ sec. and $L = 1.33$ m. (a): Nonlinear and (b) linear solutions.